HHS Public Access

Author manuscript

AJR Am J Roentgenol. Author manuscript; available in PMC 2019 October 01.

Published in final edited form as:

AJR Am J Roentgenol. 2018 October ; 211(4): 812–821. doi:10.2214/AJR.17.19462.

Diagnostic Accuracy of MRI for Detection of Papillary Renal Cell Carcinoma: A Systematic Review and Meta-Analysis

Matthew A. Chiarello[1], **Rahul D. Mali**[1], and **Stella K. Kang**[1,2]

[1]Department of Radiology, NYU School of Medicine, 550 First Ave, New York, NY 10016.

[2]Department of Population Health, NYU School of Medicine, New York, NY.

Abstract

OBJECTIVE.—The objective of our study was to perform a systematic review and meta-analysis of the diagnostic performance of MRI in differentiation of papillary renal cell carcinoma (RCC) from other renal masses.

MATERIALS AND METHODS.—We performed searches of three electronic databases for studies that used MRI techniques to differentiate papillary RCC from other renal lesions. Methodologic quality was assessed, and diagnostic test accuracy was summarized using bivariate random-effects modeling or with construction of a summary ROC (SROC) curve.

RESULTS.—Thirteen studies involving 275 papillary RCC lesions and 758 other renal masses met the inclusion criteria. Resulting summary estimates for the performance of MRI to differentiate papillary RCC from other renal lesions were a sensitivity of 79.6% (95% CI, 62.3–90.2%) and specificity of 88.1% (95% CI, 80.1–93.1%). In subgroup analysis, quantitative pooling of seven studies using enhancement in the corticomedullary phase resulted in a sensitivity of 85.6% (95% CI, 67.8–94.4%), specificity of 91.7% (95% CI, 76.0–97.5%), and area under the SROC curve of 0.894. Four studies used tumor appearance on T2-weighted imaging to detect papillary RCC, and results showed a pooled sensitivity of 89.9% (95% CI, 73.0–96.7%) and specificity of 84.9% (95% CI, 69.0–93.4%). Three studies used signal loss on T1-weighted in-phase imaging to detect papillary RCC but marked heterogeneity precluded pooling.

CONCLUSION.—Meta-analysis supports moderate sensitivity and excellent specificity of quantitative enhancement in the corticomedullary phase for differentiating papillary RCC from other tumors. The accuracy of combining enhancement and T2 signal-intensity characteristics merits further evaluation as a potential aid for management decisions.

Keywords

meta-analysis; MRI; papillary renal cell carcinoma; renal cell carcinoma; systematic review

Address correspondence to S. K. Kang (stella.kang@nyumc.org).

The content is solely the responsibility of the authors and does not necessarily represent the official views of the National Cancer Institute or the National Institutes of Health.

Based on a presentation at the Radiological Society of North America 2017 annual meeting, Chicago, IL.

Renal cell carcinoma (RCC) is composed of a heterogeneous group of histologic subtypes with variable potential to metastasize [1, 2]. Papillary RCC (in particular, type 1 papillary RCC) is generally associated with lower histologic grade, lower incidence of distant metastasis, and better cancer-specific survival than the most common RCC subtype, clear cell RCC [2]. In one large surgical series, the 5-year cancer-specific survival for clear cell RCC was 76.9%, as compared with 85.1% for papillary RCC [3].

Despite these differences among histologic subtypes in the potential to metastasize and the incidental discovery of most renal tumors at an early stage (i.e., clinical T1a), the standard of care remains surgical resection with either partial nephrectomy or nephrectomy. As alternative treatment approaches gain acceptance, noninvasive subtype differentiation may potentially help guide management decisions [4, 5]. Urologic oncologists may include the subtype information in weighing the oncologic risks of active surveillance or thermal ablation against surgery in patients with medical comorbidities or advanced age.

MRI currently serves a problem-solving role in the diagnosis of and preoperative planning for suspected RCC, particularly for discernment of enhancing soft tissue within renal lesions. In addition, unique imaging features of papillary RCC on MRI have been reported, including hypointense T2 signal, marked hypoenhancement on all phases of dynamic contrast-enhanced MRI, and signal loss on opposed-phase imaging [6, 7]. However, even among studies assessing the same MRI characteristics to diagnose papillary RCC, reported sensitivities and specificities vary widely. The summary test accuracy and potential sources of heterogeneity in reported performance characteristics remain unclear.

The body of evidence on the performance of MRI for papillary RCC detection requires systematic appraisal to drive the clinical relevance of research in this area. We therefore performed a systematic review and meta-analysis of the diagnostic accuracy of MRI in differentiation of the papillary subtype of RCC from nonpapillary renal tumors.

Materials and Methods

Literature Search

A systematic literature search of PubMed (U.S. National Library of Medicine), Embase (Elsevier), and the Cochrane Library (John Wiley & Sons) electronic databases was performed during March of 2017. The search strategy (Appendix 1) used the following terms as they appeared in the title, abstract, or keyword list and used applicable medical subject headings: renal cell carcinoma, renal mass, renal lesion, DWI, apparent diffusion coefficient, signal loss, MRI, signal intensity, papillary, differentiation, classification, and characteristics. The date of the publication was set to be as early as January 2000, and the search was updated until May 1, 2017. There was no restriction on language of publication. The resulting abstracts were then cataloged by an investigator for further analysis. Full-text articles were then reviewed for eligibility based on our inclusion criteria, and final studies for inclusion were agreed on by consensus.

Selection Criteria

We included both retrospective and prospective studies that evaluated specific MRI techniques in differentiating the papillary RCC subtype from the other RCC subtypes as well as those that distinguished papillary RCC from all other renal tumors. After initial screening of the titles and abstracts, the complete text of the relevant articles was reviewed. Articles were included if they reported sensitivity and specificity values for differentiating papillary RCC from nonpapillary renal tumors and included sufficient data for construction of 2 × 2 tables. Articles that reported the test accuracy for differentiating clear cell RCC from non–clear cell RCC, studied the separation of type 1 from type 2 papillary RCC, contained datasets that were redundant with other published studies, or assessed the differentiation of all benign from all malignant renal lesions were excluded from the study. A flowchart that shows the study selection process is presented in Figure 1.

Data Extraction

The data were extracted independently from the individual articles by two reviewers; any discrepancies were then resolved by consensus with a third reviewer. The extracted data consisted of the name of the first author, title of the study, year of publication, total number of patients, total number of lesions, number of each type of lesion (e.g., clear cell RCC, papillary RCC, angiomyolipoma), MRI protocol specifics (e.g., TR, TE, use of contrast-enhanced imaging, timing of contrast-enhanced imaging), technique of ROI measurement (where applicable), and what specific imaging parameter was measured (e.g., percentage signal intensity change, relative enhancement, apparent diffusion coefficient [ADC] value) as well as the specific cutoff values that were used for ROC analysis. The values for sensitivity, specificity, and accuracy were also recorded.

Assessment of Methodologic Quality

The methodologic quality of each study was evaluated using the Quality Assessment of Diagnostic Accuracy Studies-2 (QUADAS-2) [8]. QUADAS-2 is a tool used in systematic reviews that facilitates assessment of each individual study's potential sources of bias. The QUADAS system assesses the risk of bias and identifies applicability concerns for both the index test and the reference test of each study to be included in the systematic review. Also included are critical assessments of the patient selection techniques and the overall study design. For each assessment, the potential sources of bias have the level of risk designated as low, high, or unclear.

Data Analysis

For each individual study, the sensitivity and specificity for the detection of papillary RCC were calculated on a per-lesion basis. The bivariate random-effects model of Reitsma et al. [9] was then applied to the overall group of studies to combine data from studies for pooled sensitivity, specificity, positive likelihood ratio, and negative likelihood ratio, along with 95% CIs. The heterogeneity among studies was assessed using the chi-square statistic for the pooled estimates ($p < 0.05$, indicating significant heterogeneity). To determine whether heterogeneity could be explained at least in part by differing test thresholds for test positivity, the sensitivity and false-positive rate (FPR) were assessed for positive correlation.

The variation across studies caused by heterogeneity rather than by chance was estimated by calculating the I^2 [10]; I^2 values were defined as follows: 0–25%, heterogeneity might not be important; 26–50%, low heterogeneity; 51–75%, moderate heterogeneity; and 76–100%, high heterogeneity [11]. A Deeks funnel plot was used to assess for publication bias as indicated by an asymmetric appearance [12]. Subgroups were identified by study characteristics potentially affecting test accuracy, and sensitivity and specificity were compared for the pairwise combinations using the bivariate random-effects model. Subgroup analysis involved forest plot and pooled estimates for sensitivity and specificity using the DerSimonian-Laird random-effects model.

A summary ROC (SROC) curve was constructed for overall analysis, and the area under the SROC curve (SROC AUC) was calculated [13]. Test performance accuracy was categorized as low (SROC AUC, 0.50–0.69), moderate (0.70–0.89), or high (0.90–1.00) [14]. Statistical analysis was performed using the Meta-Analysis of Diagnostic Accuracy (i.e., mada) package within the R software (version 3.1.1, The R Foundation) environment [15] Statistical significance was determined using a p value of < 0.05.

Results

Literature Search

After the systematic review, 13 studies met the inclusion criteria and were included in the meta-analysis. The 13 studies included a total of 998 patients and 275 papillary RCC lesions for which MRI interpretation and histopathologic results were available (Appendix 2). The study characteristics of each of the included studies and the lesions evaluated in the task of separating papillary RCC from other lesion types are presented in Table 1.

Methodologic Quality

The results from the QUADAS-2 analysis are presented in Table 2. The risk of bias in patient selection was classified as unclear for six studies [4, 16–20]. Each of these studies included only patients whose pathologic confirmation was performed via surgical resection. This may have introduced bias by selecting against patients in whom watchful waiting was pursued because of small tumor size or lack of tumor growth during a period of surveillance and by favoring patients with higher histologic grade lesions or predominantly solid lesions. In terms of risk of bias related to the index test (MRI interpretation), most studies were designated low risk. One study had a potentially high risk of bias related to the index test because the interpreting radiologists were not blinded to clinical or laboratory information [4].

The reference standard, histopathologic diagnosis, showed an unclear risk of bias in eight studies [17, 20–26]. In most cases, this designation was given because the pathologic specimens in these studies were obtained via a combination of percutaneous biopsy or surgical resection. In three other studies, the reference standard had a potentially high risk of bias [4, 16, 19]. In these studies, the pathologic specimens were not independently assessed by a single pathologist; instead, the pathologic reports were reviewed and the authors did not mention whether the pathology reviewer was blinded to the imaging interpretation.

The flow and timing of patients through the study was also unclear in nine studies [4, 16–19, 21, 22, 25, 26]; these studies either did not mention the mean time between MRI and tissue sampling or did not specify the time interval between MRI and tissue sampling in the inclusion criteria [4, 16–19, 21, 22, 25, 26]. Concerns of the applicability of the index test arose as unclear in four studies [16, 18, 19, 27], two of which involved ADC measurements on 3-T scanners instead of 1.5-T scanners [18, 27] and one in which the scans were obtained on a mix of 3- and 1.5-T scanners with application of a numeric threshold for test positivity [16]. In the fourth study [19], the enhancement of the renal mass was measured on whichever sequence the interpreter determined maximum enhancement was shown; there was no standardized timed sequence to measure enhancement to enable direct comparison and reproducibility [19].

Assessment of Heterogeneity Between Studies

The 13 included studies exhibited significant heterogeneity using the chi-square statistic with p value < 0.05 for sensitivity and specificity. I^2 values showed high variability for sensitivity (84.75%) and specificity (79.13%). However, there was evidence of mild positive correlation between the sensitivity and FPR with a rho value of 0.368, suggesting the possibility that different test thresholds created a trade-off in sensitivity for specificity along a single ROC curve and an appearance of heterogeneous values.

Assessment of Publication Bias

There was evidence of asymmetry on the Deeks funnel plot (Fig. 2). Funnel plot analyses can show asymmetry for a variety of reasons other than publication bias, including the type of lesions studied and study quality, if they are linked both to sample size and observed diagnostic accuracy [28]. In this case, the two outlier studies on the right half of the plot were the only studies studying separation of papillary RCC from a comparison group containing a substantial proportion of oncocytomas or angiomyolipomas [21, 24].

Overall Diagnostic Accuracy

The summary estimates of diagnostic performance for the detection of papillary RCC using MRI were a sensitivity of 79.6% (95% CI, 62.3–90.2%) and specificity of 88.1% (95% CI, 80.1–93.1%) (Fig. 3). The partial AUC in the ROC curve of 0.819 supports overall moderate accuracy of the diagnostic test.

Subgroup Analysis: Tumor Enhancement for the Detection of Papillary Renal Cell Carcinoma

Seven of the 13 studies included relative tumor enhancement for prediction of papillary RCC and were therefore pooled quantitatively [16, 19, 20, 23–25, 27]. The pooled estimate for sensitivity was 85.6% (95% CI, 67.8–94.4%) and that for specificity was 91.7% (95% CI, 76.0–97.5%) (Fig. 4A). I^2 suggested high variability (sensitivity and specificity, 74.0, 86.4%), and the chi-square test suggested significant heterogeneity ($p < 0.05$) for sensitivity and specificity, respectively, but mild correlation between sensitivity and FPR was also seen, suggesting that a trade-off in sensitivity for specificity may partially account for

heterogeneity (ρ = 0.397). Therefore, an SROC curve was constructed, and the area under the SROC curve was 0.894 (Fig. 4B).

Subgroup Analysis: T2 Signal-Intensity Characteristics of Tumor for Detection of Papillary Renal Cell Carcinoma

Four studies assessed the use of T2 signalintensity characteristics for separating papillary RCC from other lesions (Fig. 5A). The pooled estimate for sensitivity was 89.9% (95% CI, 73.0–96.7%) and for specificity, 84.9% (95% CI, 69.0–93.4%). For sensitivities, I^2 was low (0%), and the chi-square test indicated nonsignificant heterogeneity for sensitivity (p = 0.281). For specificities, significant variability and heterogeneity were present (I^2 = 81.9%; chi-square test, $p < 0.001$), and there was strong correlation of sensitivity and FPR, suggesting a trade-off of sensitivity for specificity in ROC space (ρ = 0.699). Sensitivities and specificities are therefore presented as an SROC curve, and the SROC AUC is 0.905 (Fig. 5B).

Subgroup Analysis: Signal Loss on Opposed-Phase Imaging for Detection of Papillary Renal Cell Carcinoma

There were three studies that used signal loss on T1-weighted in-phase imaging compared with out-of-phase imaging to predict papillary RCC [17, 21, 26] (Fig. 6A). The chi-square test indicated marked heterogeneity ($p < 0.001$), and I^2 was high (sensitivity and specificity, 76.2, 86.7%). Because only two of three studies used the same quantitative measurement of signal loss (Fig. 6B), the studies' sensitivity and specificity were not quantitatively pooled.

Discussion

A meta-analysis of the diagnostic test accuracy of MRI for papillary RCC detection supports a moderate summary sensitivity of 85.6% (95% CI, 67.8–94.4%) and specificity of 91.7% (95% CI, 76.0–97.5%) using the degree of tumor enhancement to differentiate papillary RCC from nonpapillary renal lesions. In addition to thresholds of enhancement in the corticomedullary (arterial) phase, inclusion of low tumor signal intensity on T2-weighted imaging can offer moderate sensitivity (89.9%) and specificity (84.9%); therefore, the combination of these features merits further prospective evaluation for clinical application. In this way, contrast-enhanced MRI may potentially provide supplemental risk information for decision-making by predicting papillary RCC as compared with other enhancing tumors without definitive benign features, including clear cell RCC, which has an overall greater likelihood of harboring histologically aggressive potential [2]. Other MRI techniques, such as DWI, and the detection of hemosiderin or intravoxel fat on opposed-phase imaging require further investigation to assess their diagnostic added value.

Percutaneous biopsy is generally considered a safe and accurate method for determination of malignant versus benign renal masses [29]. However, the potential for non-diagnostic yield and sampling error has restricted its acceptance as a standard-of-care test for urologic oncologists, and most patients undergo nephrectomy or partial nephrectomy for small enhancing renal tumors because of the high pretest probability of RCC and overall low but heterogeneous metastatic potential of early-stage renal cancers [30, 31]. Meanwhile,

alternative treatments continue to gain increasing recognition as underlying risk factors for poor postsurgical outcomes [32–34]. When surgery is questionably beneficial as compared with potential harms, clinicians and patients may increasingly seek to incorporate more specific risk assessment to aid in treatment selection.

The relative hypovascularity of the papillary subtype of RCC differentiates it from other nonpapillary renal lesions, particularly given the typically avid enhancement seen with other solid clear cell tumors including clear cell RCC, oncocytic lesions, and angiomyolipomas. There have been several theorized mechanisms to account for the T2 hypointensity relative to renal parenchyma found in papillary RCCs, which include the presence of fibrin, hemosiderin, calcification, high nucleus-to-cytoplasm ratio, papillary architecture, and the presence of a fibrovascular stalk on histologic analysis [6, 22, 35].

To date, we are not aware of a meta-analysis of the performance of MRI in the detection of papillary RCC. Our pooled studies show significant heterogeneity among studies' sensitivities and specificities as diagnostic accuracy meta-analyses most often do [36] given nonstandardization of criteria for test positivity. However, at least some of the apparent heterogeneity in accuracy reported among studies for papillary RCC detection may be accounted for by varied thresholds determining test positivity—in particular, for thresholds of lesion contrast enhancement and T2 signal intensity.

Our study has several limitations, including the moderate quality of the literature and retrospective design of all included studies with some variability in the reference standard. In several studies, histologic diagnosis was obtained using either percutaneous biopsy or surgical resection [21, 23–25]. In three studies, only a review of the pathology reports was performed instead of a single blinded pathologist reviewing all available tissue specimens [4, 16, 19]. Study heterogeneity may be partially explained by differences in specified threshold values for test positivity; however, differences in image acquisition and quantitative image analysis may also play a role, such as the timing of contrast-enhanced phase imaging or other imaging parameters or methods of measuring the degree of tumor contrast enhancement. More uniform quantitative analysis based on timing of the contrast-enhanced phase may decrease study heterogeneity and help establish the optimal cutoff values for relative tumor enhancement. In addition, the types of lesions included in the comparator groups varied across studies, and the studies included in the meta-analysis did not address differentiation of type 1 from type 2 papillary RCC. The latter question is clinically relevant because type 2 papillary RCC may have disease-related mortality more similar to clear cell RCC than to type 1 papillary RCC [37]. Our literature search yielded two studies using MRI for differentiation of type 1 versus type 2 papillary RCC [38, 39]; these studies suggest qualitative assessment of lesion borders may be most predictive of the subtype of papillary RCC because type 2 lesions tend to appear to have ill-defined borders rather than well-circumscribed borders (as seen with type 1 papillary RCC). Still, the characteristics of type 2 papillary RCC lesions are not addressed explicitly in most of the studies in this meta-analysis, and reliable separation of papillary RCC subtypes would strengthen the utility of MRI for decision-making.

In conclusion, the moderate sensitivity and high specificity of contrast-enhanced MRI in the prediction of papillary RCC merit further evaluation as supplemental risk information for small renal tumor treatment. Prospective assessment of diagnostic test accuracy for combined features of the degree of tumor enhancement and T2 signal-intensity characteristics may help establish the utility of MRI as a noninvasive tool for aiding risk stratification and its role in decision-making for the management of small renal tumors.

Acknowledgments

S. K. Kang is supported by award number K07CA197134 from the National Cancer Institute.

APPENDIX 1:: Database Search Strategies

Database	Search Terms
PubMed (U.S. National Library of Medicine)	Renal cell carcinoma [MeSH] OR renal mass [All Fields] OR renal lesion [All Fields] AND (MRI [MeSH terms] OR DWI [All Fields] OR apparent diffusion coefficient [All Fields] OR signal intensity [All Fields] OR signal loss) AND (differentiation OR differentiate OR classification OR characterization OR characteristics)
Embase (Elsevier)	[MRI OR exp nuclear MRI] AND [papillary OR exp papillary carcinoma] AND [renal cell carcinoma OR renal mass OR renal tumor OR kidney tumor OR exp kidney carcinoma] AND [differentiation OR exp differentiation OR characterization OR exp tissue characterization] AND [histology OR exp histology OR pathology OR exp histopathology OR histologic OR diagnosis]
Cochrane Library (John Wiley & Sons)	[renal cell carcinoma] AND [papillary]

Note—MeSH = medical subject heading, exp = explode.

APPENDIX 2:: Key Imaging Parameters Extracted From the Investigated Studies

First Author [Reference No.] (Year)	TR (ms)	TE (ms)	Timing of Arterial, Nephrographic, Delayed Phases	Field Strength (T)	Relative Enhancement (%) or Enhancement Ratio	
					Arterial Phase	Nephrographic Phase
Enhancement characteristics						
Sun [25] (2009)	T2, 800–1100; T1 CSI, 180–205; T1 GRE, 3.8–4.5	T2, 60; T1 CSI, 2.2–2.7 and 4.5–5.2; T1 GRE, 1.8–2.0	First pass timed to CMD phase using a test bolus of 2 mL of contrast agent [35], and nephrographic phase initiated 20 s after CMD phase	1.5	32.1 ± 21.2[a]	96.6 ± 51.0[a]
Cornelis [24] (2014)	T2, 2112; T1 GRE, 182; dynamic GRE, 3.9; DWI, 1500	T2, 100; T1 GRE, 4.6–2.3; dynamic GRE, 1.8; DWI, 76	0, 40, 120, 250 s	1.5	0.2973[a]	0.3113[a]
Pedrosa [23] (2008)	T2, 800–1100; T1 CSI, 180–205; T1 GRE, 3.8–4.5	T2, 60; T1 CSI, 2.2–2.7 and 4.5–5.2; T1 GRE, 1.8–2.0	Timed to arterial phase and then in nephrographic phase (20 s after CMD phase)	1.5	NA	NA
Sevcenco [27] (2014)	2.88	1.44	No timing details; unenhanced, arterial (CMD), venous (nephrographic), and delayed (excretory) phases	3	77 ± 78	NA
Chandarana [20] (2012)	3.3–4.5	1.4–1.9	Acquisition delays were TTP for CMD phase, TTP plus 60 s for nephrographic phase, and TTP plus 180 s for excretory phase	1.5	55.9 ± 51.2[a] (ROI)	59.7 ± 50.4[a] (ROI)
Cupido [19] (2017)[a]	FISP, 3.6; T1 dual-phase, 136 (in-phase and out-of-phase); HASTE and fat-suppressed HASTE, infinite; VIBE, 4.3	FISP, 1.83; T1 dual-echo, 4.7 (in-phase) and 2.03 (out-of-phase); HASTE and fat-suppressed HASTE, 90; VIBE, 1.68	0, 30, 69 s	1.5	Tumor-to-cortex ratio (in whichever phase the enhancement value was maximal), 0.34 ± 0.09[b]	NA
Sasiwimonphan [16] (2012)[c]	T2, 2000–10,000; T1 GRE, 3.3–3.7	T2, 75–120; T2 GRE, 1.4–1.6	Arterial phase calculated using a 2-mL test bolus; no timing details for CMD phase; 3-min delay	1.5, 3	Arterial to delayed enhancement ratio, 1.5	NA
T2 signal-intensity characteristics						
Oliva [22] (2009)	T2, 1200–1500; T1 GRE, 260–435; 3D GRE, 4.4–7.3	T2, 87–92; T1 GRE, 4.2; 3D GRE, 1.5–2.2	No timing details	1.5	T1 SI ratios, 0.86 ± 0.23 and 0.82 ± 0.3[a]	NA
Fu [4] (2016)	Multicenter study so parameters varied		20–30, 75–80, 120–180 s	1.5	NA	NA
Signal loss on opposed-phase imaging						

First Author [Reference No.] (Year)	TR (ms)	TE (ms)	Timing of Arterial, Nephrographic, Delayed Phases	Field Strength (T)	Relative Enhancement (%) or Enhancement Ratio	
					Arterial Phase	Nephrographic Phase
Childs [26] (2014)	T2, > 3000; T1 GRE, 175–225; FSPGR, 45[d]	T2, 85; T1 GRE, 2.1–4.2; FSPGR, 4.7	20–30, 60, 90 s after bolus	1.5	NA	NA
Yoshimitsu [17] (2006)	T2, 2500; T1 GRE, 140; CSI, 150; 3D GRE, 4.2	T2, 100; T1 GRE, 4.2; CSI, 2.3; 3D GRE, 1.8	30, 90, 240 s after bolus	1.5	NA	NA
Murray [21] (2016)	55 and 64 for local MRI examinations; values varied at outside institutions		NA	1.5, 3	NA	NA
DWI						
Ponhold [18] (2016)	T2, 2000; DWI, 1700	T2, 95; DWI, 73	NA	3	NA	NA

Note—T2 = T2-weighted, T1 = T1-weighted, CSI = chemical-shift imaging, GRE = gradient-recalled echo, CMD = corticomedullary, NA = not applicable, TTP = time-to-peak, FISP = fast imaging with steady-state precession, VIBE = volumetric interpolated breath-hold examination, SI = signal intensity, FSPGR = fast spoiled gradient echo.

[a] Mean ± SD.

[b] Mean (95% CI).

[c] Also reported sensitivity and specificity for use of T2 signal-intensity characteristics to identify papillary renal cell carcinoma.

[d] The following additional sequences were performed: single-shot fast spin-echo, dual-gradient GRE, and liver acquisition with volume acceleration (LAVA, GE Healthcare).

References

1. Beck SD, Patel MI, Snyder ME, et al. Effect of papillary and chromophobe cell type on disease-free survival after nephrectomy for renal cell carcinoma. Ann Surg Oncol 2004;11:71–77 [PubMed: 14699037]
2. Cheville JC, Lohse CM, Zincke H, Weaver AL, Blute ML. Comparisons of outcome and prognostic features among histologic subtypes of renal cell carcinoma. Am J Surg Pathol 2003; 27:612–624 [PubMed: 12717246]
3. Steffens S, Janssen M, Roos FC, et al. Incidence and long-term prognosis of papillary compared to clear cell renal cell carcinoma: a multicentre study. Eur J Cancer 2012; 48:2347–2352 [PubMed: 22698386]
4. Fu W, Huang G, Moloo Z, Girgis S, Patel VH, Low G. Multimodality imaging characteristics of the common renal cell carcinoma subtypes: an analysis of 544 pathologically proven tumors. J Clin Imaging Sci 2016; 6:50 [PubMed: 28123840]
5. Campbell S, Uzzo RG, Allaf ME, et al. Renal mass and localized renal cancer: AUA guideline. J Urol 2017; 198:520–529 [PubMed: 28479239]
6. Roy C, Sauer B, Lindner V, Lang H, Saussine C, Jacqmin DM. Imaging of papillary renal neoplasms: potential application for characterization of small renal masses. Eur Radiol 2007; 17:193–200 [PubMed: 16758161]
7. Tsuda K, Kinouchi T, Tanikawa G, et al. Imaging characteristics of papillary renal cell carcinoma by computed tomography scan and magnetic resonance imaging. Int J Urol 2005; 12:795–800 [PubMed: 16201974]
8. Whiting PF, Rutjes AW, Westwood ME, et al.; QUADAS-2 Group. QUADAS-2: a revised tool for the quality assessment of diagnostic accuracy studies. Ann Intern Med 2011; 155:529–536 [PubMed: 22007046]
9. Reitsma JB, Glas AS, Rutjes AW, Scholten RJ, Bossuyt PM, Zwinderman AH. Bivariate analysis of sensitivity and specificity produces informative summary measures in diagnostic reviews. J Clin Epidemiol 2005; 58:982–990 [PubMed: 16168343]
10. Higgins JP, Thompson SG, Deeks JJ, Altman DG. Measuring inconsistency in meta-analyses. BMJ 2003; 327:557–560 [PubMed: 12958120]
11. Higgins JP, Thompson SG, Deeks JJ, Altman DG. Measuring inconsistency in meta-analyses. BMJ 2003; 327:557–560 [PubMed: 12958120]
12. Deeks JJ, Macaskill P, Irwig L. The performance of tests of publication bias and other sample size effects in systematic reviews of diagnostic test accuracy was assessed. J Clin Epidemiol 2005; 58:882–893 [PubMed: 16085191]
13. Kumar R, Indrayan A. Receiver operating characteristic (ROC) curve for medical researchers. Indian Pediatr 2011; 48:277–287 [PubMed: 21532099]
14. Swets JA. Measuring the accuracy of diagnostic systems. Science 1988; 240:1285–1293 [PubMed: 3287615]
15. Doebler, P; Mada: meta-analysis of diagnostic accuracy. r-forge.r-project.org/projects/mada/. Published 2012. Accessed December 1, 2017
16. Sasiwimonphan K, Takahashi N, Leibovich BC, Carter RE, Atwell TD, Kawashima A. Small (<4 cm) renal mass: differentiation of angiomyolipoma without visible fat from renal cell carcinoma utilizing MR imaging. Radiology 2012; 263:160–168 [PubMed: 22344404]
17. Yoshimitsu K, Kakihara D, Irie H, et al. Papillary renal carcinoma: diagnostic approach by chemical shift gradient-echo and echo-planar MR imaging. J Magn Reson Imaging 2006; 23:339–344 [PubMed: 16456822]
18. Ponhold L, Javor D, Heinz-Peer G, Sevcenco S, Hofstetter M, Baltzer PA. Inter-observer variation and diagnostic efficacy of apparent diffusion coefficient (ADC) measurements obtained by diffusion-weighted imaging (DWI) in small renal masses. Acta Radiol 2016; 57:1014–1020 [PubMed: 26486599]
19. Cupido BD, Sam M, Winters SD, et al. A practical imaging classification for the non-invasive differentiation of renal cell carcinoma into its main subtypes. Abdom Radiol (NY) 2017; 42:908–917 [PubMed: 27743018]

20. Chandarana H, Rosenkrantz AB, Mussi TC, et al. Histogram analysis of whole-lesion enhancement in differentiating clear cell from papillary subtype of renal cell cancer. Radiology 2012; 265:790–798 [PubMed: 23175544]
21. Murray CA, Quon M, McInnes MD, et al. Evaluation of T1-weighted MRI to detect intratumoral hemorrhage within papillary renal cell carcinoma as a feature differentiating from angiomyolipoma without visible fat. AJR 2016; 207:585–591 [PubMed: 27275530]
22. Oliva MR, Glickman JN, Zou KH, et al. Renal cell carcinoma: T1 and T2 signal intensity characteristics of papillary and clear cell types correlated with pathology. AJR 2009; 192:1524–1530 [PubMed: 19457814]
23. Pedrosa I, Chou MT, Ngo L, et al. MR classification of renal masses with pathologic correlation. Eur Radiol 2008; 18:365–375 [PubMed: 17899106]
24. Cornelis F, Tricaud E, Lasserre AS, et al. Routinely performed multiparametric magnetic resonance imaging helps to differentiate common subtypes of renal tumours. Eur Radiol 2014; 24:1068–1080 [PubMed: 24557052]
25. Sun MR, Ngo L, Genega EM, et al. Renal cell carcinoma: dynamic contrast-enhanced MR imaging for differentiation of tumor subtypes—correlation with pathologic findings. Radiology 2009; 250:793–802 [PubMed: 19244046]
26. Childs DD, Clingan MJ, Zagoria RJ, et al. Inphase signal intensity loss in solid renal masses on dual-echo gradient-echo MRI: association with malignancy and pathologic classification. AJR 2014; 203:[web]W421–W428 [PubMed: 25247971]
27. Sevcenco S, Ponhold L, Javor D, et al. Three-Tesla dynamic contrast-enhanced MRI: a critical assessment of its use for differentiation of renal lesion subtypes. World J Urol 2014; 32:215–220 [PubMed: 24105251]
28. Lijmer JG, Mol BW, Heisterkamp S, et al. Empirical evidence of design-related bias in studies of diagnostic tests. JAMA 1999; 282:1061–1066 [PubMed: 10493205]
29. Maturen KE, Nghiem HV, Caoili EM, Higgins EG, Wolf JS, Jr, Wood DP, Jr. Renal mass core biopsy: accuracy and impact on clinical management. AJR 2007; 188:563–570 [PubMed: 17242269]
30. Finelli A, Ismaila N, Russo P. Management of small renal masses: American Society of Clinical Oncology Clinical Practice Guideline Summary. J Oncol Pract 2017; 13:276–278 [PubMed: 28118108]
31. Yamamoto A, Tamada T, Ito K, et al. Differentiation of subtypes of renal cell carcinoma: dynamic contrast-enhanced magnetic resonance imaging versus diffusion-weighted magnetic resonance imaging. Clin Imaging 2017; 41:53–58 [PubMed: 27816876]
32. Lane BR, Campbell SC, Demirjian S, Fergany AF. Surgically induced chronic kidney disease may be associated with a lower risk of progression and mortality than medical chronic kidney disease. J Urol 2013; 189:1649–1655 [PubMed: 23201493]
33. Huang WC, Levey AS, Serio AM, et al. Chronic kidney disease after nephrectomy in patients with renal cortical tumours: a retrospective cohort study. Lancet Oncol 2006; 7:735–740 [PubMed: 16945768]
34. Kutikov A, Egleston BL, Wong YN, Uzzo RG. Evaluating overall survival and competing risks of death in patients with localized renal cell carcinoma using a comprehensive nomogram. J Clin Oncol 2010; 28:311–317 [PubMed: 19933918]
35. Shinmoto H, Yuasa Y, Tanimoto A, et al. Small renal cell carcinoma: MRI with pathologic correlation. J Magn Reson Imaging 1998; 8:690–694 [PubMed: 9626888]
36. Bossuyt PD, Deeks J, Hyde C, Leeflang M, Scholten R. Chapter 11: interpreting results and drawing conclusions
37. Mejean A, Hopirtean V, Bazin JP, et al. Prognostic factors for the survival of patients with papillary renal cell carcinoma: meaning of histological typing and multifocality. J Urol 2003; 170:764–767 [PubMed: 12913693]
38. Egbert ND, Caoili EM, Cohan RH, et al. Differentiation of papillary renal cell carcinoma subtypes on CT and MRI. AJR 2013; 201:347–355 [PubMed: 23883215]

39. Doshi AM, ReAm JM, Kierans AS, et al. Use of MRI in differentiation of papillary renal cell carcinoma subtypes : qualitative and quantitative analysis. AJR 2016; 206:566–572 [PubMed: 26901013]

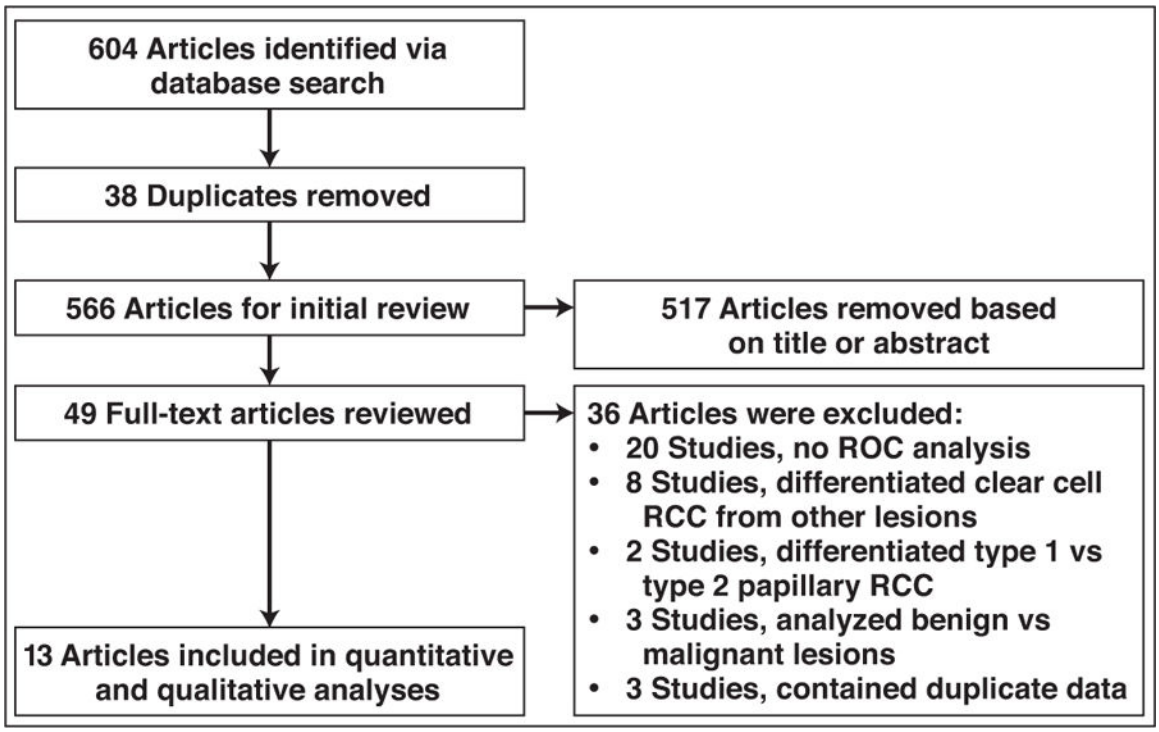

Fig. 1—.
Flowchart shows process of study selection. RCC = renal cell carcinoma.

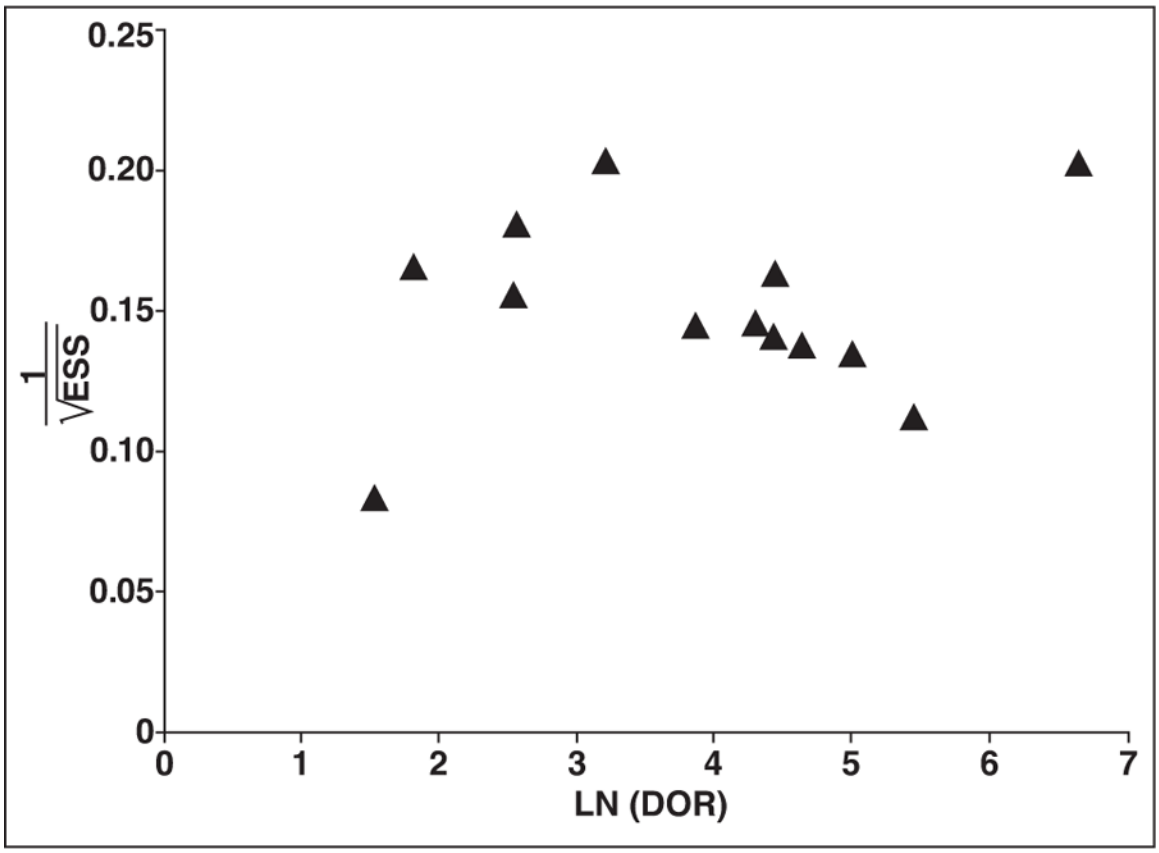

Fig. 2—.

Deeks funnel plot for assessment of publication bias, plotting log (LN) diagnostic odds ratio (DOR) against reciprocal of square root of effective sample size (ESS). Each marker represents one study included in meta-analysis. Studies with more than one technique analyzed for differentiation of papillary renal cell carcinoma from other lesions are represented only once, with preference for contrast-enhanced characteristics as technique for differentiation.

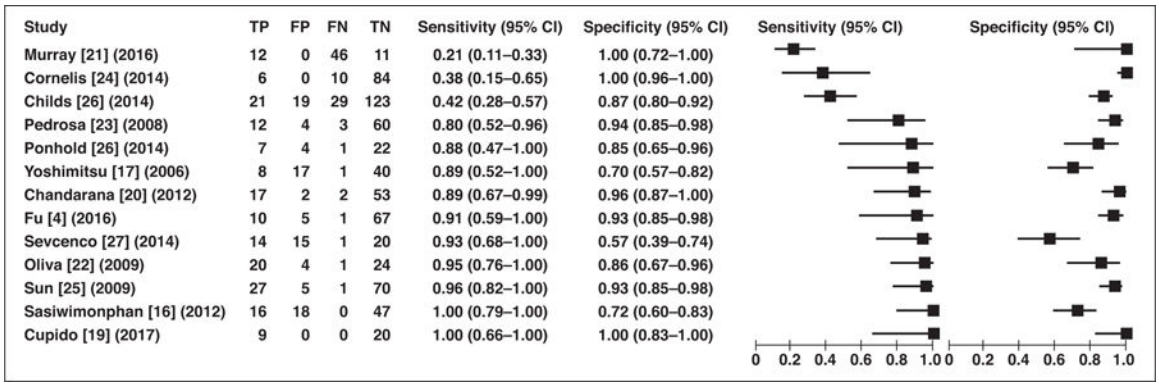

Fig. 3—.

Forest plot of sensitivity and specificity of MRI in distinction of papillary renal cell carcinoma from other types of renal masses reported in each study included in meta-analysis. Each study is identified by name of first author, reference number, and year of publication. Squares represent point estimates, and horizontal lines represent 95% CIs for sensitivity and specificity. True-positive (TP), false-positive (FP), false-negative (FN), and true-negative (TN) data are reported as number of lesions.

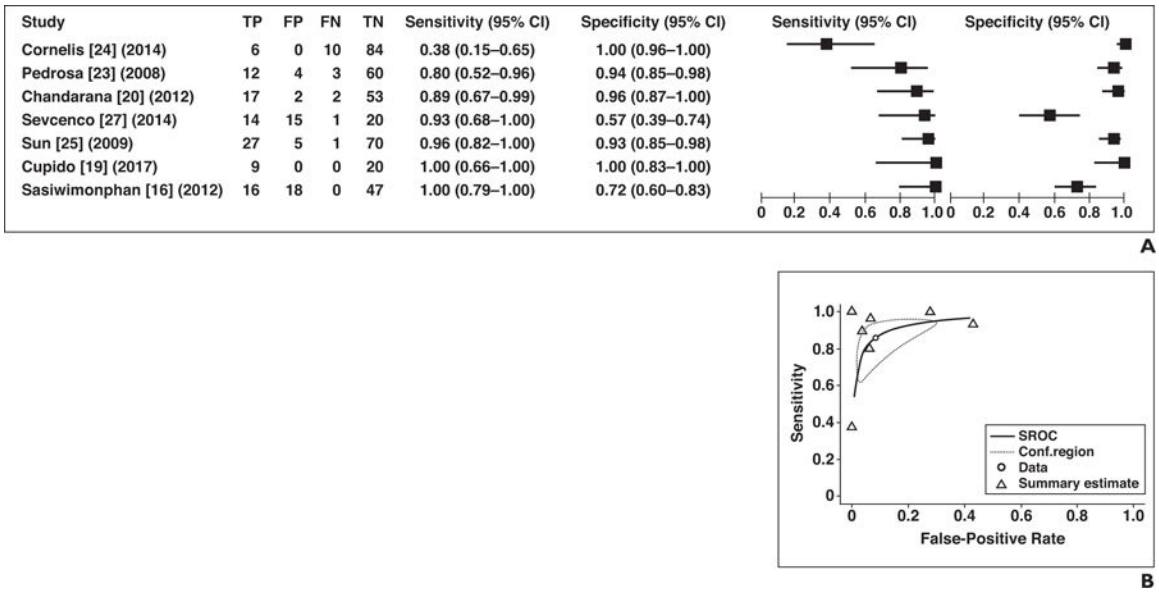

Fig. 4—. Sensitivity and specificity of seven studies that assessed relative tumor contrast enhancement for differentiation of papillary renal cell carcinoma (RCC) from other types of renal tumors.

A, Forest plot of sensitivity and specificity for investigated studies. Each study is identified by name of first author, reference number, and year of publication. Squares represent point estimates, and horizontal lines represent 95% CIs for sensitivity and specificity. True-positive (TP), false-positive (FP), false-negative (FN), and true-negative (TN) data are reported as number of lesions.

B, Summary ROC (SROC) curve of seven studies that included relative tumor contrast enhancement for differentiation of papillary RCC from other renal tumors. Area under SROC curve was 0.894. Conf.region = confidence region.

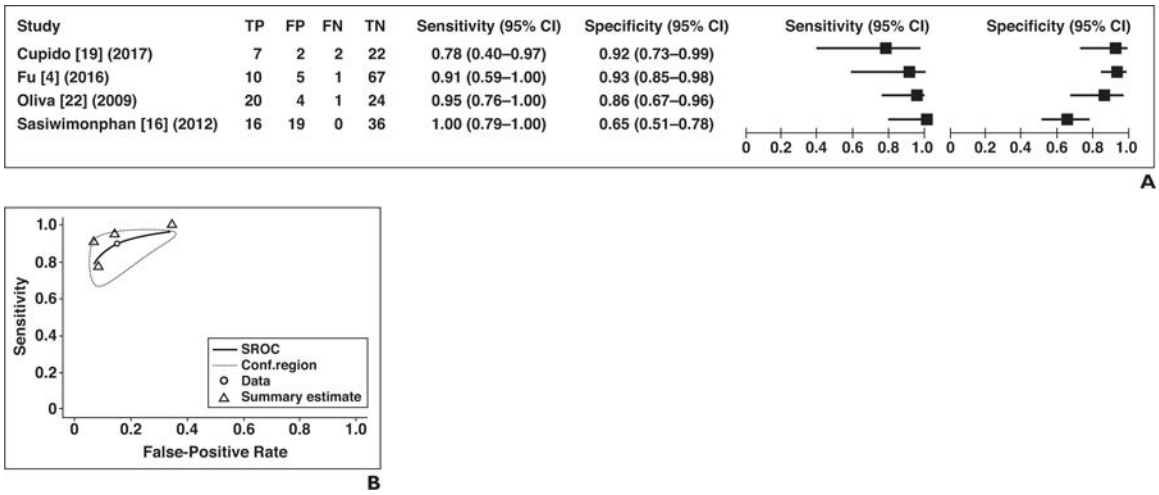

Fig. 5—. Sensitivity and specificity for studies applying T2 signal-intensity characteristics of tumor for differentiation of papillary renal cell carcinoma (RCC) from other types of renal tumors.

A, Forest plot of sensitivity and specificity for investigated studies. Each study is identified by name of first author, reference number, and year of publication. Squares represent point estimates, and horizontal lines represent 95% CIs for sensitivity and specificity. True-positive (TP), false-positive (FP), false-negative (FN), and true-negative (TN) data are reported as number of lesions.

B, Summary ROC (SROC) curve of studies that assessed use of T2 signal intensity for identification of papillary RCC presented as SROC curve. Area under SROC curve was 0.905. Conf.region = confidence region.

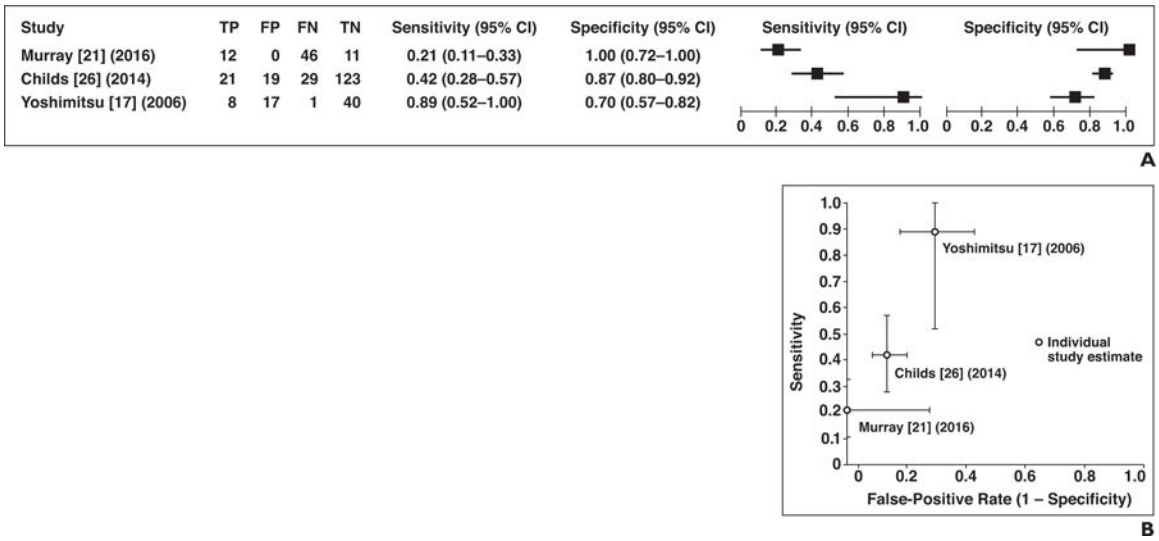

Fig. 6—. Sensitivity and specificity of studies that assessed signal loss on opposed-phase imaging for differentiation of papillary renal cell carcinoma (RCC) from other types of renal tumors.

A, Forest plot of sensitivity and specificity for investigated studies. True-positive (TP), false-positive (FP), false-negative (FN), and true-negative (TN) data are reported as number of lesions.

B, Plot of included studies in ROC space shows studies that assessed signal loss on opposed-phase imaging for identification of papillary RCC. Dots represent sensitivity and false-positive rate reported in each study and lines represent 95% CI.

AJR Am J Roentgenol. Author manuscript; available in PMC 2019 October 01.

TABLE 1:

Characteristics of Studies Included in Review and Meta-Analysis

First Author [Reference No.] (Year)	Lesions (Total No.)	Papillary RCC (No.)	Other Lesions (No.)	Types of Comparator Lesions (No. of Lesions)	Measurement of Interest	Cutoff Value	Sensitivity	Specificity
Enhancement characteristics								
Sun [25] (2009)	103	28	75	Clear cell RCC (75)	Tumor-to-cortex enhancement ratio in CMD phase	< 0.84	0.96	0.93
Cornelis [24] (2014)	100	16	84	Clear cell RCC (57), chromophobe RCC (7), oncocytoma (16), angiomyolipoma (4)	$Wil = (SI_{post} - SI_{pre}) / SI_{pre} \times 100$[a]	Wil in CMD phase < 30.9 Wil in parenchymal phase < 57.9 ADC < 54.2	0.38	1.00
Pedrosa [23] (2008)	79	15	64	Clear cell RCC (48), chromophobe RCC (5), unclassified RCC (1), TCC (7), lymphoma (2), neuroendocrine tumor (1)	MRI classification of masses into eight descriptive categories; enhancement characterization based on qualitative appearance without specifications of the phase	Category III[b] or IV[c]	0.80	0.94
Sevcenco [27] (2014)	50	15	35	Clear cell RCC (29), chromophobe RCC (6)	Peak relative enhancement of tumor on any phase: relative enhancement = SI_{post} / SI_{pre}[d]	≤ 183%	0.93	0.57
Chandarana [20] (2012)	74	19	55	Clear cell RCC (55)	Whole-lesion enhancement in CMD phase; percentage enhancement was computed on a per-voxel basis as follows: $(SI_{post} - SI_{pre}) / SI_{pre} \times 100$[d]	< 100%	0.90	0.96
Cupido [19] (2017)	29	9	20	Clear cell RCC (20)	Tumor-to-cortex enhancement ratio in CMD phase	≤ 0.55	1.00	1.00
Sasiwimonphan [16] (2012)[e]	81	16	65	Clear cell RCC (49), chromophobe RCC (4), sarcomatoid RCC with unclassifiable subtype (1), mixed clear cell and	Tumor-to-cortex enhancement ratio in CMD phase	< 1.4	1.00	0.723

First Author [Reference No.] (Year)	Lesions (Total No.)	Papillary RCC (No.)	Other Lesions (No.)	Types of Comparator Lesions (No. of Lesions)	Measurement of Interest	Cutoff Value	Sensitivity	Specificity
				papillary RCC (1), angiomyolipoma (10)				
T2 signal-intensity characteristics								
Oliva [22] (2009)	49	21	28	Clear cell RCC (28)	T2 signal intensity ratio (compared with cortex)	≤ 0.93	0.952	0.857
Cupido [19] (2017)	33	9	24	Clear cell RCC (20), chromophobe RCC (4)	T2 signal intensity	Low T2 signal intensity	0.778	0.917
Fu [4] (2016)	83	11	72	Clear cell RCC (67), chromophobe RCC (5)	T2 signal intensity	Low T2 signal intensity	0.91	0.93
Sasiwimonphan [16] (2012)[e]	71	16	55	Clear cell RCC (49), chromophobe RCC (4), sarcomatoid RCC with unclassifiable subtype (1), mixed clear cell and papillary RCC (1)	T2 signal intensity ratio (compared with cortex)	< 1.0	1.00	0.655
Signal loss on opposed-phase imaging								
Childs [26] (2014)	192	50	142	Clear cell RCC (102), chromophobe RCC (4), mixed subtype (7), unclassified RCC (2), sarcomatoid clear cell (1), lymphoproliferative disorder (1), UCC (1), poorly differentiated carcinoma (1), malignant oncocytoid (1); benign lesions (22 [including 3 angiomyolipomas, 17 oncocytomas, 2 others])	Signal loss index = $[Signal_{in} - Signal_{out}] / Signal_{out}$[f]	≤ –0.03	0.48	0.83
Yoshimitsu [17] (2006)	66	9	57	Clear cell RCC (57)	Signal loss ratio = $[Signal_{in} - Signal_{out}] / Signal_{in}$[g]	< –0.1	0.89	0.70
Murray [21] (2016)	69	58	11	Angiomyolipoma (11)	Signal intensity index of loss = $[Signal_{in} - Signal_{out}] / Signal_{out} \times 100$[h]	< –16%	0.21	1.00

First Author [Reference No.] (Year)	Lesions (Total No.)	Papillary RCC (No.)	Other Lesions (No.)	Types of Comparator Lesions (No. of Lesions)	Measurement of Interest	Cutoff Value	Sensitivity	Specificity
DWI								
Ponhold [18] (2016)	34	8	26	Clear cell RCC (21), chromophobe RCC (3), TCC (2)	ADC	$\leq 990 \times 10^{-6}$	0.88	0.85

Note—RCC = renal cell carcinoma, CMD = corticomedullary, WiI = wash-in index, ADC = apparent diffusion coefficient, TCC = transitional cell carcinoma, UCC = urothelial cell carcinoma.

[a] Where WiI is the wash-in index, SI_{post} is the signal intensity on contrast-enhanced images, and SI_{pre} is the signal intensity on unenhanced images.

[b] Category III = hemorrhagic cystic masses with peripheral enhancing projections (predicts high-grade papillary RCC).

[c] Category IV = small homogeneous masses of low signal intensity in T2-weighted images (predicts low-grade papillary RCC).

[d] Where SI_{post} is the signal intensity on contrast-enhanced images and SI_{pre} is the signal intensity on unenhanced images.

[e] Lesion-level data in the development set of this study can be used to calculate a 2 × 2 table for differentiating papillary RCC from other RCC subtypes and angiomyolipomas using tumor enhancement ratio and T2 signal intensity ratio. The subgroup analysis on tumor enhancement characteristics for differentiation of papillary RCC from other lesions includes minimal-fat angiomyolipoma as a type of comparator lesion. For the analysis of T2 signal-intensity characteristics for differentiation of papillary RCC from other lesions, the sensitivity and specificity presented are without angiomyolipomas in the comparator group to reduce heterogeneity among studies in this small subgroup.

[f] Where $Signal_{in}$ is the signal intensity on in-phase imaging and $Signal_{out}$ is the signal intensity on opposed-phase imaging.

[g] Where $Signal_{in}$ is the signal intensity on in-phase imaging and $Signal_{out}$ is the signal intensity on opposed-phase imaging.

[h] Where $Signal_{in}$ is the signal intensity on in-phase imaging and $Signal_{out}$ is the signal intensity on opposed-phase imaging.

TABLE 2:

Quality Assessment of Included Studies: Summarized Risk of Bias and Applicability

First Author [Reference No.] (Year)	Risk of Bias				Applicability Concerns		
	Patient Selection	Index Test	Reference Standard	Flow and Timing	Patient Selection	Index Test	Reference Standard
Sun [25] (2009)	Low	Low	Unclear	Unclear	Low	Low	Low
Cornelis [24] (2014)	Low	Low	Unclear	Low	Low	Low	Low
Pedrosa [23] (2008)	Low	Low	Unclear	Low	Low	Low	Low
Sevcenco [27] (2014)	Low	Low	Low	Low	Low	Unclear	Low
Chandarana [20] (2012)	Unclear	Low	Unclear	Low	Unclear	Low	Low
Cupido [19] (2017)	Unclear	Low	High	Unclear	Unclear	Unclear	Low
Oliva [22] (2009)	Low	Unclear	Unclear	Unclear	Low	Low	Low
Childs [26] (2014)	Low	Low	Unclear	Unclear	Low	Low	Low
Ponhold [18] (2016)	Unclear	Low	Low	Unclear	Low	Unclear	Low
Murray [21] (2016)	Low	Low	Unclear	Unclear	Low	Low	Low
Yoshimitsu [17] (2006)	Unclear	Unclear	Unclear	Unclear	Low	Low	Low
Fu [4] (2016)	Unclear	High	High	Unclear	Low	Low	Low
Sasiwimonphan [16] (2012)	Unclear	Low	High	Unclear	Unclear	Unclear	Low